

Uncovering the neutrino mass ordering with the next galactic core-collapse supernova neutrino burst using water Cherenkov detectors

César Jesús-Valls^{1,*}

¹*Kavli IPMU (WPI), UTIAS, The University of Tokyo, Kashiwa, Chiba 277-8583, Japan*

A major conundrum of particle physics is what mass ordering (MO) follow neutrinos. Due to matter effects the flavor content of the neutrino flux from a Core-Collapse Supernovae (CCSNe) is expected to be highly dependent on the true neutrino MO. In this article, the potential to uncover the true neutrino MO using CCSN neutrinos and water Cherenkov detectors is studied. A novel analysis strategy is presented, designed to be robust to all existing systematic uncertainties and readily applicable to the Super-Kamiokande or Hyper-Kamiokande experiments. The results show that for a paradigmatic CCSN at 10 kpc, Hyper-Kamiokande might discriminate the true neutrino MO with a confidence similar to 2-3 σ . In the case of a nearby CCSN at a radius of 3.5 kpc (1 kpc) from Earth, Hyper-Kamiokande (Super-Kamiokande) would reach a sensitivity beyond 5 σ .

I. INTRODUCTION

Neutrinos are essential ingredients of particle physics, astrophysics and cosmology, yet, some of their fundamental properties remain unknown. Under the most extended theoretical picture, consisting on the existence of three neutrino flavors able to mix, neutrino phenomenology is characterized by a set of seven parameters divided into three neutrino masses (m_1, m_2 and m_3) and four mixing parameters ($\theta_{12}, \theta_{23}, \theta_{13}$ and δ_{CP}). Currently, $\theta_{12}, \theta_{23}, \theta_{13}, \delta m_{21}^2 (\equiv m_2^2 - m_1^2)$ and $|\Delta m_{32}^2| (\equiv |m_3^2 - m_2^2|)$ are known with few percent precision [1, 2] such that only three quantities remain elusive: a) the absolute neutrino mass scale, e.g. review [3], b) the value of δ_{CP} , e.g. refs. [2, 4] and c) the sign of Δm_{32}^2 , i.e. the so-called neutrino mass ordering (MO) that can be normal $m_2 < m_3$ (NMO) or inverted $m_3 < m_2$ (IMO).

Regarding the MO, current data shows a statistical preference for the NMO of about 3σ [2]. Future experiments Hyper-Kamiokande [5], JUNO [6] and DUNE [7] will characterize the MO in detail via the study of atmospheric, reactor and accelerator neutrino oscillations. The complementarity of the above experiments is an attractive advantage: if all the MO results are consistent, it will reinforce the existing view of neutrino phenomenology, while the appearance of tensions in data could give us hints of new physics [8–10] requiring theoretical extensions. In the second scenario, having additional data would be particularly helpful in disentangling the true MO of new physical effects. In this sense, a unique opportunity would arise in the event of a galactic supernova (SN) neutrino burst [11–13].

A. Supernova neutrino bursts

Core collapse supernovae (CCSN) emit $O(10^{53})$ erg as neutrinos, i.e. $O(10^{58})$ neutrinos of $\langle E_\nu \rangle \sim 10$ MeV,

in a ten-second burst [14, 15]. A low galactic rate of 1.63 ± 0.46 CCSN per century is expected [16]. Consequently, so far only a couple dozen neutrinos have been detected from a single supernova, SN-1987a [17–20]. Nonetheless, the detection of SN-1987a confirmed our basic understanding of CCSN explosions and signified the start of experimental neutrino astrophysics. Furthermore, since the predicted neutrino flux and flavor composition are greatly influenced by a plethora of effects, the SN-1987a data was used to place significant limits on several exotic processes [21–25] and properties of neutrinos, including their mass [26, 27], magnetic moment [28] and mixing [29]. These achievements, however, are just a tantalizing hint of what might be possible with next-generation neutrino detectors. The increase of available data would be spectacular, e.g. $O(10^{4-6})$ detected neutrinos at Hyper-Kamiokande for a burst at a distance of 10-1 kpc [5]. Such a drastic improvement, however, would pose new challenges, in particular, the decrease in statistical error would force to shift the analysis focus towards the treatment and evaluation of systematic uncertainties, so far overlooked, in order to get the most from the precious supernova data.

B. Experimental prospects: DUNE, Super-Kamiokande and Hyper-Kamiokande

Among future experiments, DUNE is mainly sensitive to the ν_e flavor, such that the (non-)observation of the so-called neutronization peak in the first milliseconds of the explosion would naturally constitute strong evidence of the IMO (NMO) [12]. Notably, the emission in this initial stage of the explosion is also the best understood from a phenomenological stand-point and therefore this analysis strategy can also be considered robust [12, 30]. In contrast, water Cherenkov detectors are mainly sensitive to the $\bar{\nu}_e$ flavor and consequently, the identification of the neutronization peak would require a more intricate analysis exploiting the angular distribution of the final

* E-mail: cesar.jesus-valls@ipmu.jp

state leptons, as highlighted in the Hyper-Kamiokande design report [31], in order to be able to discriminate the contribution of different neutrino flavors. This article is the first to present a detailed analysis strategy that aims to assess the neutrino MO using water Cherenkov detectors while paying attention to all sources of systematic uncertainty. With it, the expected MO sensitivities for Super-Kamiokande and Hyper-Kamiokande detectors are reported. The value of this study lies in that:

- In the occurrence of a CCSN, the analysis strategy here presented could be readily applied to Super-Kamiokande data or to Hyper-Kamiokande data if the explosion happens after 2027.
- Until the DUNE experiment becomes operational in the 2030s, water Cherenkov detectors provide the best MO sensitivity from CCSN data. If a CCSN occurs once DUNE and Hyper-Kamiokande are online, both results could be combined or used as a cross-check.
- The reported sensitivity factors in the most relevant uncertainties and therefore provides a meaningful estimate of what sensitivity could be achieved using the existing and planned water Cherenkov detectors.

C. Neutrino flux predictions

The explosion mechanism of CCSN is still poorly understood [32]. However, the gradual increase in available computational power has allowed the set of simplifying assumptions to be reduced over time, and in recent years CCSN models have begun to achieve realistic self-triggered explosions [32]. Furthermore, a general concordance has emerged in the neutrino flux predictions from different research teams [33–37].

New data from a future CCSN would be game-changing to better understand the dynamics of the explosion and to assess the reliability of the available models. Recently, first studies have shown that great CCSN model-discrimination could be achieved using Hyper-Kamiokande [5] (HK) or a HK-like detector [38]. This results might be potentially complemented with similar studies in JUNO [39] and DUNE [30] in the future.

D. Flavor transformations

During the neutronization burst or shock period, i.e. the first $\lesssim 50$ ms [12], the matter potential is expected to be dominant over the neutrino-neutrino potential and consequently flavor transformations are expected to be described by the standard MSW effect [5, 12, 30, 40, 41]. If $\sin^2 \theta_{13} > 10^{-3}$, as it is indeed the case [42], a non-oscillatory adiabatic flavor conversion, sensitive to the neutrino MO, is expected [43]. At later times, $50 \lesssim$

$t \lesssim 200$ ms [12], during the so-called accretion phase and along the cooling phases, describing the remaining part of the burst, other effects such as SASI (standing accretion shock instability), turbulences, and neutrino self-interactions, might play a significant role, altering in non-trivial and not well understood manners the flavor composition of the flux [32, 44–47].

E. Relevant interaction cross-sections

Supernova neutrinos have typical energies at the level of few tens of MeV [20]. At such energies, the main interactions with detector targets consists of neutrino- and antineutrino-electron elastic scattering (eES) [48], electron antineutrino inverse beta decay (IBD) [49] with unbound protons such as Hydrogen in water, and neutrino-nucleon charged- and neutral-current interactions with bound nucleons (e.g. ν_e -CC ^{16}O [50, 51]). Due to nuclear effects, neutrino interactions with bound nucleons are poorly known [52, 53], instead, eES and IBD predictions are expected to be accurate.

II. ANALYSIS STRATEGY

The analysis strategy consists in: 1) identifying an observable at water Cherenkov detectors that is sensitive to the neutrino flux flavor composition 2) define an event selection criteria 3) estimate the total systematic uncertainty and 4) calculate the sensitivity to the neutrino MO using the former inputs.

A. Flux models

To study different flux models the SNEWPY [54, 55] open-source software package is used. The models under consideration are, following SNEWPY's nomenclature, **Bollig 2016** ($27 M_{\odot}$) [56], **Warren 2020** ($13 M_{\odot}$) [57] **Fornax 2021** ($20 M_{\odot}$) [32], **Zha 2021** ($16 M_{\odot}$) [58]. This choice aims to use relatively new models, less tied to simplifying assumptions than earlier models, spanning a wide range of progenitor masses. To account for flavor transformations the neutrino flux predictions are modified according to **AdiabaticMSW** transformationsⁱ using SNEWPY. These transformations depend on θ_{13} and θ_{23} [11], with values chosen from the Particle Data Group [59]. Since the uncertainty on these parameters is small the variations inflicted to the expected flavor predictions are minor, specially when compared to CCSN model-to-model variations. Hence, the uncertainty on these parameters is neglected, such as in Ref. [5].

ⁱ Implementation details are available in Appendix A of Ref. [54].

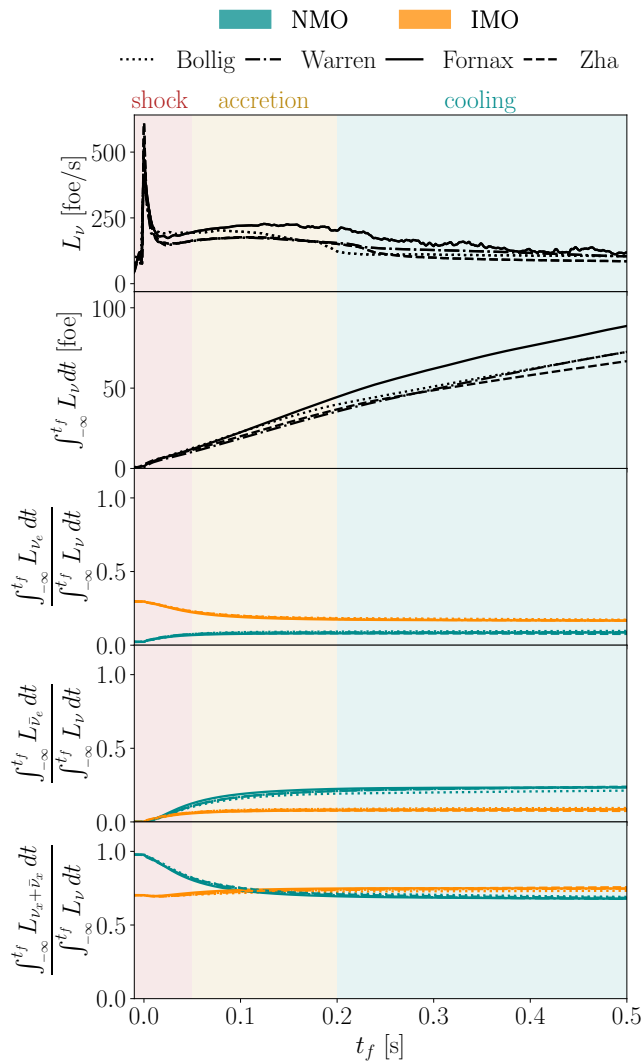


FIG. 1: From top to bottom: Neutrino luminosity, cumulative total luminosity, cumulative fraction of the ν_e flavor, cumulative fraction of the $\nu_{\bar{e}}$ flavor and cumulative fraction of the $\nu_x + \nu_{\bar{x}}$ flavor as functions of time. The cumulative luminosities are integrated from the start of the SN explosion, denoted by $-\infty$, until a time, t , for the different flux models presented in the text. The different phases of the explosion are denoted by color shades.

Neutrino flux models, see Fig. 1, have the neutrino luminosity divided into four flavor categories: L_{ν_e} , $L_{\bar{\nu}_e}$, L_{ν_x} and $L_{\bar{\nu}_x}$, where $x \equiv \mu + \tau$. The time evolution of the supernova explosion is markedly different between models such that $L(t)$ is not a model-robust observable. This is also true for the total neutrino luminosity integrated over time, i.e., $\int L_{\nu}(t) dt$ due to, among other effects, scale differences, e.g. the progenitor mass. However, as presented in see Fig. 1, the time-integrated fraction of different flavors is consistently different as a function of the true neutrino MO across flux models.

Since each model uses a different time reference definition, small time offsets are applied by setting the t_0 of each model as the time at which the neutrino luminosity reaches its maximum. Notably, this time frame could also be set for data analyzing the time spectrum of events. Although this calculation would introduce an associated detector systematic uncertainty, its role is later neglected as it would be, arguablyⁱⁱ, a sub-leading correction.

B. Observable definition

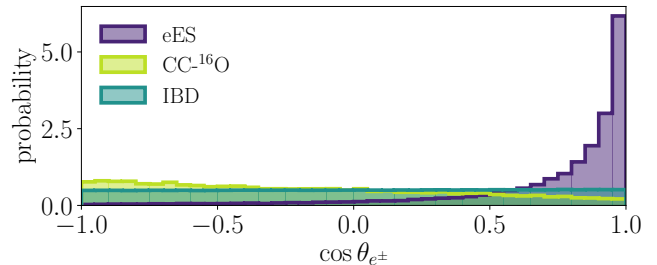


FIG. 2: Binned probability density function of the reconstructed angle for outgoing electrons and positrons, split by interaction channel, generated for neutrino interactions in water using the **Warren** flux model, presented in the text, transformed by **AdiabaticMSW** for the NMO.

To be sensitive to the MO, it is necessary to find an observable that changes with the flux flavor content such that the differences presented in the former section can be sized. Among the interaction channels listed in Sec. IE all flavors contribute equally to eES whereas IBD is only possible for $\bar{\nu}_e$. Therefore, a measurement able to discriminate one reaction from the other is directly informative of the flux flavor and therefore of the true neutrino MO. It is well known that electrons emitted in eES are peaked forward whereas those from IBD and CC- ^{16}O are almost isotropic, as illustrated in Fig. 2. This feature has been used for years in the study of solar neutrinos [60] and provides the best known strategy to reconstruct the CCSN position in the sky [31]. Here, this feature is used to study the neutrino MO by noting that the expected shape of the angular distribution of outgoing e^{\pm} is strongly influenced by the flux flavor content and therefore by the true neutrino MO. To be insensitive to the flux model-to-model time and normalization variations presented in Fig.1 time information is used exclusively to selected events detected in the first 50 ms, i.e.

ⁱⁱ If a low number of interactions is recorded, statistical errors dominate. Else, σ_{t_0} could be determined precisely, and a small time offset would translate into a minor variation of the integrated flavor composition, due to the small flavor gradients in the cumulative distributions observed at around 50 ms in Fig. 1.

associated to the neutronization phase, and the resulting angular distribution is normalized to unity. Therefore, the analysis sensitivity is based on the shape-only variation of the angular distribution of outgoing e^\pm induced by the true MO.

C. Super-Kamiokande and Hyper-Kamiokande

Super-Kamiokande, 25 kT of fiducial mass, is currently the existing world reference of water Cherenkov neutrino detectors. Hyper-Kamiokande, 187 kT of fiducial mass, is being built nearby and it is expected to take over in 2027. The reconstruction performance of Super-Kamiokande is very well understood as Super-Kamiokande has been operating for nearly three decades. The performances of Hyper-Kamiokande are expected to match or supersede those of Super-Kamiokande [31]. Therefore, to simulate detector effects in both Super-Kamiokande and Hyper-Kamiokande the reconstructed lepton energy and angle are smeared using the reconstruction performances reported by the solar neutrino analysis of Super-Kamiokande IV [60].

D. Event simulation and selection criteria

To translate neutrino luminosities into event rates the `sntools` [61] open-source software package is used. `sntools` reads fluxes in SNEWPY format and combines them with neutrino cross-sections to generate realistic event rates and particle distributions using Monte Carlo sampling.

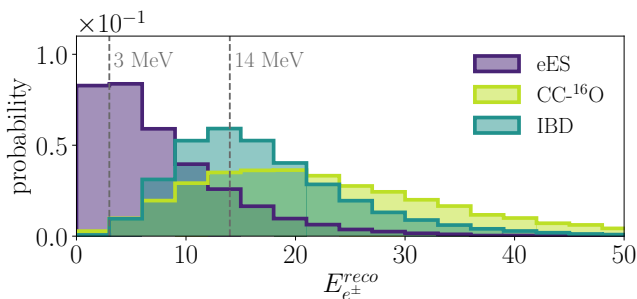


FIG. 3: Binned probability density function of the reconstructed energy for outgoing electrons and positrons, split by interaction channel, generated for neutrino interactions in water using the Warren flux model, presented in the text, transformed by AdiabaticMSW for the NMO.

Over half a million events are simulated for each SN model and MO and the expected normalized angular distribution of the outgoing e^\pm is computed relative to the SN direction. The true θ_{e^\pm} and E_{e^\pm} are smeared according to Super-Kamiokande IV performances [60]. Then, events with $E^{max} > E_{e^\pm}^{reco} > 3$ MeV are selected. This

Cuts	NMO			IMO		
	IBD [%]	eES [%]	^{16}O [%]	IBD [%]	eES [%]	^{16}O [%]
A	87.6±0.6	9.4±0.9	3.1±1.3	86.1±1.1	10.7±0.7	3.2±1.4
B	89.7±0.7	7.1±0.7	3.2±1.3	88.5±1.1	8.2±0.5	3.3±1.4
C	84.6±0.4	13.09±0.6	1.5±0.3	74.2±2.1	23.5±1.6	2.3±0.6

TABLE I: Fractions of selected interactions in HK after applying the cuts A, B and C , corresponding to: A) No cuts; B) $E_{e^\pm}^{reco} > 3$ MeV and C) $14 > E_{e^\pm}^{reco} > 3$ MeV. The intervals reflect the mean and standard deviation of the values found across the flux models in Sec. II A.

choice aims to: 1) account for a realistic detection energy thresholdⁱⁱⁱ and 2) increase (decrease) the fraction of eES (CC- ^{16}O), which is concentrated at low (high) energies, see Fig. 3, and reduce the flux model-to-model discrepancies, particularly relevant at high $E_{e^\pm}^{reco}$. While aggressive cuts on E^{max} improve the model robustness, they reduce the number of selected events and therefore increase the statistical error. To balance such a trade-off, $E^{max} = 14$ MeV was chosen as it provides maximum MO sensitivity^{iv}. After the cuts, the interaction fractions change as summarized in Tab. I. The cuts significantly reduce decrease the fraction of CC- ^{16}O and significantly increase the proportion of eES events. As intended, the separation of NMO and IMO predictions is significantly accentuated by using a high-energy cut.

E. Evaluation of uncertainties

To account for the cross-section model uncertainties, the weight associated to all selected CC- ^{16}O is varied assuming a 100% normalization uncertainty^v. For each MO and toy configuration, i.e., a particular instance of a flux model, collection of smeared angles and energies, and cross-section weights the resulting normalized angular distribution is calculated. The mean of all distributions and its standard deviation corresponds to the expected angular distribution and its associated uncertainty. This is presented in the top panel of Fig. 4. To get some insight on the nature of the total error budget the size of individual contributions is studied. To quantify the role of detector uncertainties all cross-section weights are set to one and calculated individually for each flux model. The flux-averaged detector uncertainty (det) is calculated as the mean of the spreads

ⁱⁱⁱ In SK-IV a threshold as low as 3.49 MeV was used to study solar neutrinos [60]. Hyper-Kamiokande expects to detect 10 photo-electrons/MeV compared to the 6 photo-electrons/MeV at SK-IV [62]. Thus, a 3 MeV threshold is assumed.

^{iv} The whole analysis chain was re-run to test several values of E^{max} , in steps of 1 MeV.

^v The absence of experimental data prevents the use of a more specific choice. The value of 100% is a usual conservative choice when a normalization constrain is missing.

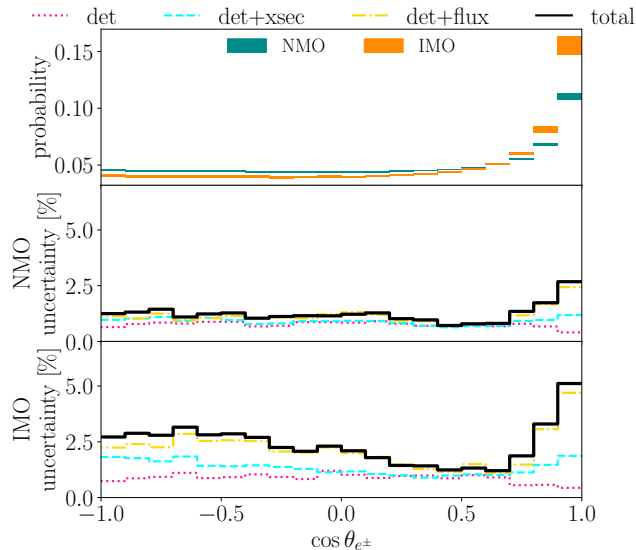


FIG. 4: Binned probability of the expected angular distribution for both MOs. Each bin is represented as a colorbox covering 1σ of the total uncertainty. Central and bottom panels: break-down of the uncertainty for each MO in terms of its detector-only (*det*), detector and cross-section (*det+xsec*), and detector and flux (*det+flux*) systematic uncertainties.

across flux models. The process is repeated, this time varying at the same time the cross-section weights, leading to a detector plus cross-section uncertainty averaged across flux models (*det+xsec*). Finally, the cross-section weights are set to one, and the variation across detector effects and flux models (*det+flux*) is calculated. It is worth noting that, since reconstructed variables are used, cross-section and flux model uncertainties are intertwined with detector effects and, consequently, *det+xsec* and *det+flux* are reported together. The results are presented in the central and bottom panels of Fig. 4. The dominant contribution is that of flux model differences followed by cross-section effects.

In the future, it might be possible to shrink the flux and cross-section uncertainties if: 1) The SN explosion mechanism is better understood and the results of different groups continue to converge and 2) model predictions for low energy, i.e. $O(10)$ MeV, neutrino-nucleus interactions can be compared to data. The state-of-the-art of neutrino research, very active on both of the former topics, makes it possible to expect updates in the near future.

The statistical uncertainty (σ_{stat}) can be straightforwardly computed distributing a number of selected neutrinos, N^{sel} , according to the distributions in the top panel of Fig. 4 and sizing the variations using Poisson statistics. To calculate the total error budget the statistical and systematic uncertainties (σ_{syst}) are added in quadrature ($\sigma_{stat} \oplus \sigma_{syst}$).

F. Sensitivity calculation

The sensitivity corresponds to the statistical separation between both MOs. To calculate it, the following method is used:

- A MO is assumed, i.e., the NMO.
- A number of selected SN neutrino interactions, N^{sel} , is chosen.
- A set of 50k toys are generated. Each toy corresponds to sample Gaussianly the value of each bin from the assumed MO mean and total uncertainty.
- For each toy, χ_{NMO}^2 and χ_{IMO}^2 are calculated using

$$\chi_M^2 = \sum_i^{bins} \frac{(\mu^i - \hat{\mu}_M^i)^2}{\sigma_M^2}, \quad \chi_M^2 = \{\chi_{NMO}^2, \chi_{IMO}^2\} \quad (1)$$

where $\hat{\mu}_M^i$, μ^i and σ_M^i are respectively the expected value, the toy value and the uncertainty at the i -th bin for the mass ordering M .

- $\Delta\chi^2$ is calculated, defined as $\Delta\chi^2 \equiv \chi_{NMO}^2 - \chi_{IMO}^2$.
- The distribution of $\Delta\chi^2$ for all toys is fit with a Gaussian. By, definition, positive (negative) values are indicative of the NMO (IMO). To obtain the sensitivity of correctly assessing the MO the fit is integrated from $-\infty$ to 0. Finally, the p-value is converted into σ .

III. SENSITIVITY AND OUTLOOK

Using the above method the sensitivity to identify the true MO is calculated for a number of selected neutrinos in the interval from 0 to 8k. The results are presented in Fig. 5. To isolate the contribution of systematic uncertainties, the results are presented both for σ_{stat} only and for $\sigma_{stat} \oplus \sigma_{syst}$. To provide some intuition on the expected number of selected neutrinos as a function of different CCSN distances from Earth, vertical color bands are included. Each color band covers the region from the minimum to the maximum number of expected selected neutrinos at Super-Kamiokande or Hyper-Kamiokande for the flux models under consideration for different CCSN distances.

The results show that for Super-Kamiokande, only nearby CCSN would allow to have some sensitivity, similar to $2-3\sigma$ at 3 kpc and surpassing the 5σ level exclusively at distances of about 1 kpc. A much better scenario can be expected for Hyper-Kamiokande, where even at the typical galactic distance of 10 kpc a notable sensitivity of $2-3\sigma$ is reached. For CCSN closer than 3.5 kpc Hyper-Kamiokande would discriminate both orderings with a confidence beyond 5σ .

Interestingly, the results show that the sensitivity is

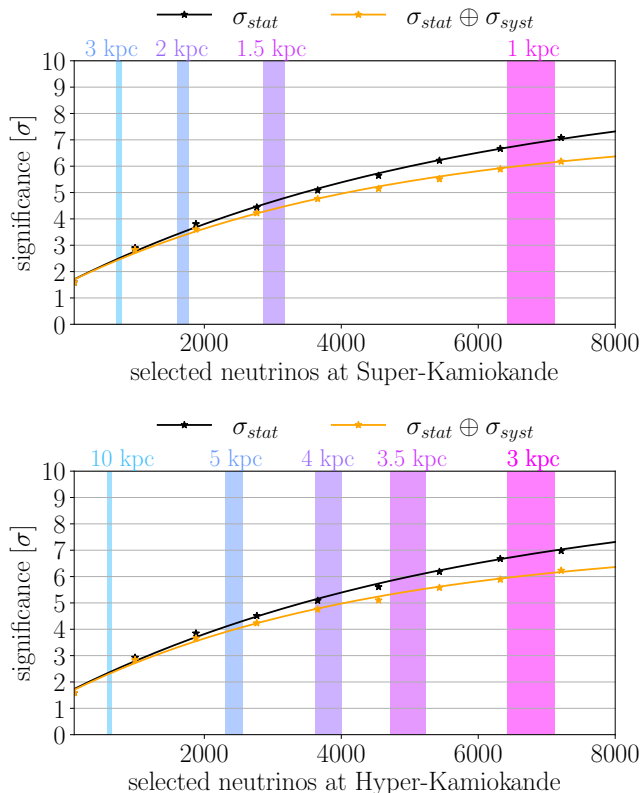


FIG. 5: Sensitivity to the true neutrino MO as a function of the number of neutrinos selected at Super-Kamiokande (top) and Hyper-Kamiokande (bottom) with the criteria discussed in the text. The color bands show the interval covering the number of expected selected neutrinos event assuming the NMO for all models used in the analysis at different CCSN distances from Earth.

mainly limited by statistical errors. Increasing the time window to include the accretion and cooling phases of the explosion can easily counterbalance this shortcoming and would dramatically increase the sensitivity. However, in order to include that data without compromising the robustness of the results still requires further theoretical progress and a better understanding of the CCSN explosion.

Summing up, the results show that: 1) the time-integrated flavor content is a flux-model robust quantity indicative of the true neutrino MO; 2) the shape of the normalized angular distribution of outgoing e^\pm is a scale-robust sensible observable to study the flavor composition of a SN neutrino flux; 3) The Super-Kamiokande and Hyper-Kamiokande detectors are a well suited technology for that analysis thanks its excellent pointing capabilities and its large mass; 4) the current level of systematic uncertainties affects the shape-only predictions at the few percent level; 5) for typical galactic distances of 10 kpc Super-Kamiokande would not be able to infer the neutrino MO whereas Hyper-Kamiokande would achieve a notable sensitivity, similar to 2-3 σ . In the serendipitous event of a nearby CCSN, Super-Kamiokande (Hyper-Kamiokande) would be able to uncover the true neutrino MO if the explosion would happen within a radius of about 1 kpc (3.5 kpc) from Earth.

ACKNOWLEDGMENTS

The author is indebted to CERN for organizing the INSS where the idea of this project was first sparked and acknowledges fruitful discussions with T. Lux, E. Ramos-Cascón and P. Barham, the help of J. Migenda to install SNEWPY and `sntools` and the feedback on the manuscript from C. Alt, S. Dolan and S. Julià-Farré.

-
- [1] P. F. de Salas, D. V. Forero, S. Gariazzo, P. Martínez-Miravé, O. Mena, C. A. Ternes, M. Tórtola, and J. W. F. Valle, *JHEP* **02**, 071 (2021), arXiv:2006.11237 [hep-ph].
 - [2] I. Esteban, M. C. Gonzalez-Garcia, M. Maltoni, T. Schwetz, and A. Zhou, *JHEP* **09**, 178 (2020), arXiv:2007.14792 [hep-ph].
 - [3] J. A. Formaggio, A. L. C. de Gouvêa, and R. G. H. Robertson, *Phys. Rept.* **914**, 1 (2021), arXiv:2102.00594 [nucl-ex].
 - [4] K. Abe *et al.* (T2K), *Nature* **580**, 339 (2020), [Erratum: *Nature* 583, E16 (2020)], arXiv:1910.03887 [hep-ex].
 - [5] K. Abe *et al.* (Hyper-Kamiokande), *Astrophys. J.* **916**, 15 (2021), arXiv:2101.05269 [astro-ph.IM].
 - [6] F. An *et al.* (JUNO), *J. Phys. G* **43**, 030401 (2016), arXiv:1507.05613 [physics.ins-det].
 - [7] B. Abi *et al.* (DUNE), (2020), arXiv:2002.03005 [hep-ex].
 - [8] P. B. Denton, J. Gehrlein, and R. Pestes, *Phys. Rev. Lett.* **126**, 051801 (2021), arXiv:2008.01110 [hep-ph].
 - [9] S. S. Chatterjee and A. Palazzo, *Phys. Rev. Lett.* **126**, 051802 (2021), arXiv:2008.04161 [hep-ph].
 - [10] P.-W. Chang, I. Esteban, J. F. Beacom, T. A. Thompson, and C. M. Hirata, (2022), arXiv:2206.12426 [hep-ph].
 - [11] A. S. Dighe and A. Y. Smirnov, *Phys. Rev. D* **62**, 033007 (2000), arXiv:hep-ph/9907423.
 - [12] K. Scholberg, *J. Phys. G* **45**, 014002 (2018), arXiv:1707.06384 [hep-ex].
 - [13] V. Brdar and X.-J. Xu, *JCAP* **08**, 067 (2022), arXiv:2204.13135 [hep-ph].
 - [14] S. W. Barwick *et al.*, (2004), arXiv:astro-ph/0412544.
 - [15] H.-T. Janka, *Ann. Rev. Nucl. Part. Sci.* **62**, 407 (2012), arXiv:1206.2503 [astro-ph.SR].
 - [16] K. Rozwadowska, F. Vissani, and E. Cappellaro, *New Astron.* **83**, 101498 (2021), arXiv:2009.03438 [astro-ph.HE].
 - [17] K. Hirata *et al.* (Kamiokande-II), *Phys. Rev. Lett.* **58**, 1490 (1987).

- [18] K. S. Hirata *et al.*, Phys. Rev. D **38**, 448 (1988).
- [19] R. M. Bionta *et al.*, Phys. Rev. Lett. **58**, 1494 (1987).
- [20] H. A. Bethe, Rev. Mod. Phys. **62**, 801 (1990).
- [21] G. Raffelt and D. Seckel, Phys. Rev. Lett. **60**, 1793 (1988).
- [22] M. S. Turner, Phys. Rev. Lett. **60**, 1797 (1988).
- [23] G. G. Raffelt, Lect. Notes Phys. **741**, 51 (2008), arXiv:hep-ph/0611350.
- [24] J. H. Chang, R. Essig, and S. D. McDermott, JHEP **01**, 107 (2017), arXiv:1611.03864 [hep-ph].
- [25] J. H. Chang, R. Essig, and S. D. McDermott, JHEP **09**, 051 (2018), arXiv:1803.00993 [hep-ph].
- [26] J. N. Bahcall and S. L. Glashow, Nature **326**, 476 (1987).
- [27] D. N. Spergel and J. N. Bahcall, Phys. Lett. B **200**, 366 (1988).
- [28] R. Barbieri and R. N. Mohapatra, Phys. Rev. Lett. **61**, 27 (1988).
- [29] B. Jegerlehner, F. Neubig, and G. Raffelt, Phys. Rev. D **54**, 1194 (1996), arXiv:astro-ph/9601111.
- [30] B. Abi *et al.* (DUNE), Eur. Phys. J. C **81**, 423 (2021), arXiv:2008.06647 [hep-ex].
- [31] K. Abe *et al.* (Hyper-Kamiokande), (2018), arXiv:1805.04163 [physics.ins-det].
- [32] A. Burrows and D. Vartanyan, Nature **589**, 29 (2021), arXiv:2009.14157 [astro-ph.SR].
- [33] E. J. Lentz, S. W. Bruenn, W. R. Hix, A. Mezzacappa, O. E. B. Messer, E. Endeve, J. M. Blondin, J. A. Harris, P. Marronetti, and K. N. Yakunin, Astrophys. J. Lett. **807**, L31 (2015), arXiv:1505.05110 [astro-ph.SR].
- [34] T. Melson, H.-T. Janka, and A. Marek, Astrophys. J. Lett. **801**, L24 (2015), arXiv:1501.01961 [astro-ph.SR].
- [35] M. A. Skinner, J. C. Dolence, A. Burrows, D. Radice, and D. Vartanyan, Astrophys. J. Suppl. **241**, 7 (2019), arXiv:1806.07390 [astro-ph.IM].
- [36] E. P. O'Connor and S. M. Couch, Astrophys. J. **865**, 81 (2018), arXiv:1807.07579 [astro-ph.HE].
- [37] T. Kuroda, A. Arcones, T. Takiwaki, and K. Kotake, Astrophys. J. **896**, 102 (2020), arXiv:2003.02004 [astro-ph.HE].
- [38] J. Olsen and Y.-Z. Qian, Phys. Rev. D **105**, 083017 (2022), arXiv:2202.09975 [astro-ph.HE].
- [39] T. Birkenfeld (JUNO), PoS **ICHEP2020**, 619 (2021).
- [40] S. P. Mikheyev and A. Y. Smirnov, Sov. J. Nucl. Phys. **42**, 913 (1985).
- [41] L. Wolfenstein, Phys. Rev. D **17**, 2369 (1978).
- [42] P. A. Zyla *et al.* (Particle Data Group), PTEP **2020**, 083C01 (2020).
- [43] A. Y. Smirnov, Phys. Scripta T **121**, 57 (2005), arXiv:hep-ph/0412391.
- [44] R. F. Sawyer, Phys. Rev. D **72**, 045003 (2005), arXiv:hep-ph/0503013.
- [45] H. Nagakura, L. Johns, A. Burrows, and G. M. Fuller, Phys. Rev. D **104**, 083025 (2021), arXiv:2108.07281 [astro-ph.HE].
- [46] I. Padilla-Gay, I. Tamborra, and G. G. Raffelt, Phys. Rev. Lett. **128**, 121102 (2022), arXiv:2109.14627 [astro-ph.HE].
- [47] H. Nagakura, A. Burrows, D. Vartanyan, and D. Radice, Monthly Notices of the Royal Astronomical Society **500**, 696 (2021).
- [48] J. N. Bahcall, M. Kamionkowski, and A. Sirlin, Phys. Rev. D **51**, 6146 (1995), arXiv:astro-ph/9502003.
- [49] A. Strumia and F. Vissani, Phys. Lett. B **564**, 42 (2003), arXiv:astro-ph/0302055.
- [50] T. Suzuki, S. Chiba, T. Yoshida, K. Takahashi, and H. Umeda, Phys. Rev. C **98**, 034613 (2018), arXiv:1807.02367 [nucl-th].
- [51] K. Nakazato, T. Suzuki, and M. Sakuda, PTEP **2018**, 123E02 (2018), arXiv:1809.08398 [astro-ph.HE].
- [52] N. Van Dessel, A. Nikolakopoulos, and N. Jachowicz, Phys. Rev. C **101**, 045502 (2020), arXiv:1912.10714 [nucl-th].
- [53] S. Gardiner, Phys. Rev. C **103**, 044604 (2021), arXiv:2010.02393 [nucl-th].
- [54] A. L. Baxter *et al.* (SNEWS), Astrophys. J. **925**, 107 (2022), arXiv:2109.08188 [astro-ph.IM].
- [55] A. Baxter *et al.*, J. Open Source Softw. **6**, 3772 (2021).
- [56] A. Mirizzi, I. Tamborra, H.-T. Janka, N. Saviano, K. Scholberg, R. Bollig, L. Hudepohl, and S. Chakraborty, Riv. Nuovo Cim. **39**, 1 (2016), arXiv:1508.00785 [astro-ph.HE].
- [57] M. L. Warren, S. M. Couch, E. P. O'Connor, and V. Morozova, Astrophys. J. **898**, 139 (2020), arXiv:1912.03328 [astro-ph.HE].
- [58] S. Zha, E. P. O'Connor, and A. da Silva Schneider, Astrophys. J. **911**, 74 (2021), arXiv:2103.02268 [astro-ph.HE].
- [59] M. Tanabashi *et al.* (Particle Data Group), Phys. Rev. D **98**, 030001 (2018).
- [60] K. Abe *et al.* (Super-Kamiokande), Phys. Rev. D **94**, 052010 (2016), arXiv:1606.07538 [hep-ex].
- [61] J. Migenda, S. Cartwright, L. Kneale, M. Malek, Y.-J. Schnellbach, and O. Stone, J. Open Source Softw. **6**, 2877 (2021).
- [62] J. Bian *et al.* (Hyper-Kamiokande), in *2022 Snowmass Summer Study* (2022) arXiv:2203.02029 [hep-ex].